

# **CHAPTER 3. MODELING DECADAL BED-MATERIAL SEDIMENT FLUX BASED ON STOCHASTIC HYDROLOGY**

(Submitted)

## **Abstract**

This paper reports estimates of decadal bed-material sediment flux and net storage obtained by driving sediment transport calculations with a stochastic hydrology model. The resulting estimates represent the whole distribution of sediment flux based on the natural variability in channel characteristics (gradient, width, and bed grain size), and the magnitude, duration, and interarrival time of flood events. The paper describes a procedure for calibrating common sediment transport formulae to the bed-material grain-size distribution at a cross section. The procedure is applied to the Sacramento River basin to compute estimates of annual total and annual peak bed-material discharges into and through the mainstem over a thirty-year period. Simple mainstem bed-material budgets are evaluated to identify reaches in states of net accumulation or scour. Simulations highlight large imbalances in sediment storage throughout the Sacramento River, which can be explained by a combination of local hydraulics and bed material grain size distributions.

## **Introduction**

Bed-material flux is the transport of sediment that is present in a riverbed and is available for transport by streamflow. The variability in bed-material flux

throughout a river channel results in spatial patterns in sediment storage. These storage patterns influence the formation of the channel (e.g. point bars) and its functioning (e.g. depth of flow over an portion of a cross section). Accordingly, sediment storage can be thought of as a first-order determinant of habitat conditions in a river reach.

Long-term estimates of bed-material sediment flux and net storage in large rivers are required for various purposes ranging from applications in flood control (bed elevations) and river rehabilitation to research on sediment budgets and channel morphology. These estimates are generally reported as single values derived from sediment transport data with no assessment of the uncertainty in their calculation (e.g. [Milliman and Meade, 1983; Milliman and Syvitski, 1992]) or their inter-annual variation. Dunne *et al.* [1998] applied error propagation to sediment rating curve analyses of sediment fluxes and reach accumulations in the Amazon basin. But to my knowledge, there are limited methods available for representing inter-annual variability in load estimates due to a variable flow regime. Toward this end, I have calibrated a sediment transport formula with measurements from the Sacramento and other rivers, and connected it to HYDROCARLO, a stochastic model of streamflow [Singer and Dunne, Submitted]. I used the coupled models to estimate the probability distributions, including the extrema and central tendency, of bed-material discharge in various grain-size classes over a period of decades. I have applied this method at various cross sections along the mainstem Sacramento River and at the mouth of its

major tributaries, and thus developed a basinwide method for assessing the long-term influence of flood variability on bed-material transport.

Many studies have acknowledged the inaccuracies in sediment transport prediction arising from uncertainty in hydraulic variables [*McLean*, 1995], spatial distribution of bed shear stress [*Wilcock*, 1996], and assessment of critical shear stress [*Buffington and Montgomery*, 1997]. However, flow is an additional source of uncertainty introduced when one tries to obtain a decadal estimate of bedload flux. For even if one could properly constrain each of the aforementioned variables for a given set of flow conditions, it would still be necessary to properly characterize the stochastic frequency, magnitude, and duration of flow at a given cross-section, in order to obtain an appropriate estimate of long-term bed-material flux. Such a strategy is particularly important to determining the role of floods in sediment transport and channel formation, and for assessing riverine habitat condition.

Long-term sediment flux prediction that incorporates the real variability inherent in a fluvial system would be useful on the scale of a cross section where computations are made (e.g. to evaluate local adjustment to a rehabilitation strategy) and that of a basin as a whole (e.g. to assess the influence of system-wide perturbations on the sediment budget). In order to design a gravel augmentation strategy on the local scale, for example, it would be useful to quantify the central tendency and extrema of spawning-sized gravel transport past a particular cross section. On the basin scale, it would be useful to assess the influence of land-use change (e.g. an increase in sand loading to the channel) on bed-material transport in

various grain sizes throughout the mainstem. This paper outlines a basinwide method for quantifying the variations in bed-material transport over a period of decades punctuated by flood events of variable frequency, magnitude, duration, drawdown rate, and interarrival time.

I built this method using data from the Sacramento River basin in California. I perform the following at mainstem and tributary cross sections along the Sacramento River: 1) stochastically simulate daily flow for 30 years [*Singer and Dunne*, Submitted]; 2) simplify cross-sectional geometry and calculate hydraulic variables for distinct portions of the cross section; 3) obtain the grain-size distribution from bulk material surveys; 4) determine dimensionless critical shear stress from bedload data; 5) modify a common sediment transport formula to incorporate local critical shear stress, fractional transport prediction, and prediction in distinct portions of a cross section; 6) calibrate the modified equation to various bedload data; 7) calibrate the modified equation to the grain-size distribution of the local bed-material; 8) simulate daily bedload flux for 30 years in various grain size classes; 9) combine long-term bedload estimates with my prior estimates of long-term suspended sediment discharge [*Singer and Dunne*, 2001] at mainstem locations to evaluate the contribution of bedload to total load; and 10) construct simple bed-material sediment budgets (annual total and one-day peak values) for reaches of the Sacramento fluvial system.

## **Study Basin**

The Sacramento River basin is approximately 70,000 km<sup>2</sup> in drainage area and the river flows from its headwaters near Mount Shasta through the northern Central Valley to the San Francisco Bay-Delta in California. It is controlled at the northern end by Shasta Dam, which was built in 1943. The Sacramento spans a range of fluvial environments. From Shasta Dam, it winds southward through Sacramento Canyon, incises into Pleistocene deposits on the Redding plain, and bends through Iron Canyon to Bend Bridge (BB in Figure 3.1). This part of the river, called Reach 0 (Figure 3.1) in this study, is ~40 km in length, consists of a mixed bed (~28% sand in bed-material at BB), width of ~150 m, slope of  $\sim 8.9 \times 10^{-4}$  and has point bar topography. South of Bend Bridge the Sacramento enters the Central Valley, where it meanders across a wide floodplain through Pleistocene river gravels to Hamilton City (HC). Reach 1 is ~60 km in length, consists of a gravel and sand bed (~40% sand at HC), width of ~200 m and slope of  $\sim 5.4 \times 10^{-4}$ , with shallow cross sections characterized by ~2 m natural levees. Below Hamilton City the Sacramento continues meandering through the valley, but is partially constrained by flood control levees, which influence the river's course upstream of Butte City (BC). Reach 2 is ~30 km in length, consists of similar bed-material (~49% sand at BC), cross-sectional topography, and width as Reach 1, but with a lower slope ( $\sim 2.5 \times 10^{-4}$ ). Below Butte City the Sacramento enters a reach where flood control levees are set back ~1 km from the channel until Colusa (CO). Reach 3 is ~25 km in length, consists of a sand bed (~75% sand at CO), width and cross sectional topography similar to the upstream reaches, and a slope of  $\sim 2.3 \times 10^{-4}$ . It is controlled at the downstream end by an

eastward deflection around the Colusa Dome, which forces sequestration of water and deposition of sediment [*Singer and Dunne, 2001*]. Downstream of Colusa the Sacramento is incised into the Pleistocene deposits of the Cache Creek fan and is completely constrained by flood control levees built on channel banks to Knights Landing (KL). Reach 4 is ~55 km in length, consists of a sand bed (~73% sand at KL) with lenses of gravel, width of ~100 m, largely symmetrical cross sections, and slope of  $\sim 1.0 \times 10^{-4}$ . The Sacramento River below Knights Landing continues south to Sacramento (SA), where the river is influenced by tides. Reach 5 is ~30 km in length, consists of a sand bed (99% sand at SA)  $\sim 0.8 \times 10^{-4}$ .

I compute sediment discharge at cross sections that bound these river reaches and directly correspond with gauging stations for which I previously made long-term estimates of suspended sediment transport [*Singer and Dunne, 2001*]. Most cross sections used in this study have fixed widths over the range of moderate-to-high flows due to combinations of flood control levees, riprap, and revetment.

The tributaries of the Sacramento flow from four geologic provinces, each of which is assumed to deliver a uniform sediment yield per unit drainage area. I compute bed-material transport into the Sacramento from each tributary in a unit by computing the load for a signature tributary on the province and scaling it by the ratio of drainage areas for the remaining tributaries. The signature tributaries for this study are Cottonwood Creek, Cow Creek, Thomas Creek, and Feather River, draining the Trinity Mountains, Modoc Plateau, Coast Ranges, and Sierra Nevada, respectively.

## **Data**

I employ channel cross sections extracted from high-resolution (0.7 m contours) digital terrain models of the mainstem Sacramento provided by the US Army Corps of Engineers (USACE) and the California Department of Water Resources (CDWR). These datasets were obtained by bathymetric surveys in 1997 and 2000, respectively. Together, they form a seamless set of contemporaneous (within 3 years) cross sections through which flow routing and sediment transport may be computed. Flow data from the Sacramento's major tributary gauges were obtained from the US Geological Survey (USGS) as described in [*Singer and Dunne*, Submitted]. To define grain-size distributions and calibrate sediment transport formulae, I use bedload and suspended load data from USGS gauging stations, and bed-material grain-size distributions from the USGS and CDWR bulk material surveys.

## **Stochastic Hydrology Model**

In order to drive the sediment transport calculations, I developed a stochastic hydrology model that simulates inflow to the mainstem of a large river from its major tributaries by semi-random sampling of tributary flood events. The model, HYDROCARLO [*Singer and Dunne*, Submitted], produces synchronous inflow from tributaries by replicating empirical patterns in flood occurrence and correlation in flood peak magnitude between tributary gauges. In applying it to the Sacramento River basin, I demonstrated the overwhelming influence of basinwide storms that

induce synchronous flood conditions at all tributary gauges. I also showed that the model produces plausible patterns of tributary inflow which, when routed through the mainstem produce hydrographs with characteristics (e.g. peak, duration, interarrival time) similar to those of observed mainstem hydrographs.

In the sediment transport study, I used HYDROCARLO to simulate daily inflow to the mainstem Sacramento River for a 30-year period that represents the hydrology of the era since the construction of Shasta Dam. I routed this inflow through the mainstem to each of the selected cross sections (Figure 3.1) using the flow routing software, HEC-RAS, and extracted mean daily flow stage for the duration of each 30-year simulation. I conducted 50 such simulations to stochastically represent a large range of flood events in the basin and to converge on extrema and central tendency of bedload flux associated with them.

## **Cross-Sectional Geometry and Hydraulics**

Bedload flux may differ in distinct portions of a river channel cross section due to differences in flow depth that lead to spatial variability in shear stress [Wilcock, 1996]. For example, shear stresses are higher in the thalweg than on a high bar surface (Figure 3.2), if the bed-material grain-size distribution is spatially uniform. Therefore, calculating rates of sediment transport for an entire cross-section based on mean flow depth could introduce inaccuracies into the results. I have simplified the geometry for each of my cross sections to represent the varying depths that could lead to differential transport rates in distinct portions of the section based

on a single cross-sectional stage. I divided cross-sections into portions, each with its own elevation datum and width (Figure 3.2).

I used daily flow elevation extracted from HEC-RAS to compute daily water surface slope,  $s$ , for the cross-section as a whole as

$$s_x = \frac{\left( \frac{z_{x+1} - z_x}{c_1} + \frac{z_x - z_{x-1}}{c_2} \right)}{2} \quad (1)$$

where  $z$  is water surface elevation, the subscripts  $x$ ,  $x+1$ , and  $x-1$  denote the cross section average of the section in question, the next upstream section, and the next downstream section, respectively,  $c_1$  is the centerline distance between sections  $x+1$  and  $x$ , and  $c_2$  is the centerline distance between sections  $x$  and  $x-1$ . Centerline distances between cross sections are  $\sim 800$  m. Hereafter I refer to section average quantities with the subscript  $x$  and quantities for a portion of the cross section with the subscript  $p$ . Flow depth for a portion of the cross section,  $h_p$ , is calculated by subtracting the bed elevation of that portion,  $z_p$ , from the water surface elevation for the section as a whole,  $z_x$ . I used the resulting flow depths,  $h_p$ , and the section-average water surface slope,  $s_x$ , from (1) to compute mean daily velocity for each portion of the cross section using the Manning equation:

$$v_p = \frac{h_p^{2/3} s_x^{1/2}}{n_x} \quad (2)$$

where  $v$  is velocity,  $n$  is the Manning's roughness coefficient. I obtained constant Manning's roughness values for each cross section from prior hydraulic calibrations of bathymetric datasets by USACE and CDWR. Next I calculated bed shear stress for each portion of a section,  $\tau_p$ :

$$\tau_p = \rho g h_p s_x \quad (3)$$

where  $\rho$  is the density of water (assumed to be  $1000 \text{ kg/m}^3$ ) and  $g$  is gravitational acceleration. In other words, I am making the approximation that all flow is parallel to the banks and bed. I converted shear stress to its dimensionless form [Shields, 1936]:

$$\tau_p^* = \frac{\tau_p}{(\rho_s - \rho) g d_{50_x}} \quad (4)$$

where  $\tau^*$  is dimensionless shear stress (i.e. Shields stress),  $\rho_s$  is density of sediment (assumed to be  $2650 \text{ kg/m}^3$ ), and  $d_{50}$  is median grain size of the bed material, obtained for each section from bulk material sampling [California Dept. of Water

*Resources*, 1994]. Lateral characterization of dimensionless shear stress (i.e. across the channel) could be improved by higher resolution bulk surveys of bed material, which would provide median grain size for each portion of the cross section,  $d_{50p}$ . This may particularly important in cases where there is marked lateral sorting of bed sediments (e.g. sections with coarse bars and fine pools).

### **Bed-material Grain Size**

Correct specification of sediment grain size is necessary in order to obtain realistic predictions of sediment flux because of the sensitivity of sediment transport equations to grain size distribution. For example, washload (i.e. that part of the sediment load which is not present on the riverbed) should not be computed with an equation designed to predict transport of bed material. The grain size range of a particular transport mode can be defined operationally as that which can be caught in a particular sampler (e.g. [Edwards and Glysson, 1999]). The Helley-Smith bedload sampler [Helley and Smith, 1971] has been shown to be 100% effective in trapping grain sizes between 0.5 and 16 mm for a 75 mm intake (or 32 mm with a 150 mm intake) [Emmett, 1980]. Although particles as fine as 0.2 mm can be physically caught by the Helley-Smith, the mode of their transport is uncertain [Emmett, 1980]. The DH-series, depth-integrated suspended sediment sampler is statistically effective at capturing sediment ranging from 0.001 to 0.5 mm in diameter [Edwards and Glysson, 1999], traveling within 75 mm of the bed.

I compared grain-size distributions for bed material, suspended load, and bedload (for stations that had such data) collected for mainstem Sacramento River stations between 1977 and 1980 (Figure 3.3). These data show that 0.5 mm is an approximate lower limit grain size for bed material at most stations in the basin. Grain sizes larger than 0.5 mm are present in less than 5% of suspended load samples and more than 5% of bed material samples in the gravelly reaches. These factors indicate that 0.5 mm is the natural separation between washload and bed-material transport (whether bedload or suspended load) for the Sacramento basin. The sand-bed reaches at Butte City, Knights Landing, and Sacramento, have 0.25 mm as their lower limit (Figure 3.3c, e, and f). Suspended sediment is almost entirely comprised of washload in the Sacramento (Figure 3.3) and its tributaries. The exceptions are the Sacramento station and the Feather River station (Figure 3.1), where fine-grained bed material mostly moves in suspension. However, for the remaining sections, there are two populations of sediment moving in distinct transport modes. Herein I model bed-material discharge with the assumption that there is no overlap between them. I compute sediment discharge for up to nine grain size classes,  $i$ , ( $d_{50i}$  (mm) = 0.38, 0.75, 1.5, 3, 6, 12, 24, 48, and 96). However, at the lower end of the distribution, I limit the computations to grain sizes that constitute less than 5% of the suspended load at a given cross section. This is particularly important because I employ a sediment transport equation designed only for bed material transport calculations (see below).

## Critical Shear Stress

Recent research in gravel transport has emphasized the importance of characterizing the threshold of incipient motion to ensure that sediment transport is not predicted in cases where the threshold for movement is not met. More than a threefold range in this threshold arises from the condition of the bed (e.g. grain shape, size, and packing, pocket angle). Numerous methods have been developed over eight decades of research [Buffington and Montgomery, 1997] to compute dimensionless critical shear stress,  $\tau_c^*$ , and it is common practice to employ a characteristic value (e.g.  $\tau_c^* = 0.047$  for gravel) when local transport data are unavailable. However, in cases where bedload data are available, it is preferable to compute the local threshold value. This has been commonly done by a technique called similarity collapse originally developed in Japan [Ashida and Michiue, 1972; Parker *et al.*, 1982].

Parker, *et al.* [1982] plotted dimensionless transport rate against dimensionless shear stress in each grain size class. They fitted a curve to the data within each grain size class and extended this curve down to a reference transport rate of 0.002 to obtain a reference shear stress, or a surrogate of the dimensionless critical shear stress for that grain size. They plotted these dimensionless reference shear stresses against the ratio of the median grain size (of each bedload size class) to the median grain size of the bed subsurface. This yielded a power relationship with a coefficient that approximates the dimensionless critical shear stress,  $\tau_c^*$ , for incipient motion of the entire mixture.

However, the current study is not concerned with incipient motion of sediments. It is instead concerned with defining a threshold for sediment transport that can be measured with a bedload sampler. Therefore, I compute  $\tau_c^*$  as the lowest Shields stress,  $\tau_x^*$ , that yields transport for the lowest observed bedload rate. In other words, I obtain  $\tau_c^*$  by adjusting its value until excess shear stress (i.e.  $\tau_x^* - \tau_c^*$ ) is positive for the hydraulic conditions of the lowest measured transport rate where both sand and gravel were in motion. This approach is especially useful to define a transport threshold in cases where a scarcity of bedload measurements leads to difficulties in defining the relationship between dimensionless transport and dimensionless shear stress. For one station where I had ample bedload data (Bend Bridge, Figure 3.1), the similarity collapse yielded  $\tau_c^* = 0.040$  and my method yielded  $\tau_c^* = 0.053$ . Table 3.1 provides information for each station including  $\tau_c^*$ , drainage area, and median bed-material grain size.

## **Sediment Transport Equation Modification and Calibration**

Previous researchers have computed sediment transport with formulae calibrated to specific laboratory and/or field data. Many such formulae have been extensively reviewed (e.g. [*White et al.*, 1975; *Gomez and Church*, 1989]). The equations that *Gomez and Church* [1989] found to be most accurate (*Bagnold and Parker, et al.*) were extensively calibrated on the best available measurements of bedload in gravel-bed rivers. Most shear stress-based sediment transport equations are of a similar form [*Gomez and Church*, 1989], e.g. containing an excess shear

stress term, or a ratio or difference of computed shear stress and critical shear stress raised to some power. Therefore, I reason that it matters less, which equation is used, but how well a particular equation can be calibrated to predict sediment transport in a particular river system. This is especially important because sediment transport computed with commonly-used equations may predict rates a factor of 2-10 times observed bedload rates, particularly for the highest recorded values. Until the theory of sediment transport improves to represent the range of laboratory flume and field sediment transport conditions, there is little utility in applying specific empirical equations to a new place without recalibrating to local transport data, if they exist. Although such a practice has merit in studies investigating the applicability of particular equations (e.g. [Andrews, 1981; Batalla, 1997]), it has limited use in long-term prediction of sediment transport rates. Here I demonstrate that prediction of sediment transport rates in a particular place can be improved by calibrating one of a number of commonly-used sediment transport formulae to local bedload and bed material data and simulating over a range of hydraulic conditions.

For this study, I have chosen the Engelund-Hansen formula [Engelund and Hansen, 1967; Vanoni, 1975] for total load. The original equation was developed by relating sediment transport to excess shear stress and bed friction using data from flume experiments on a dune-covered sandy bed [Guy *et al.*, 1966]. It has had reasonable success in predicting sediment transport in a variety of sand and gravel environments (e.g. [White *et al.*, 1975; Yang and Wan, 1991; Reid and Dunne, 1996; Batalla, 1997]). In their calibration of the equation, Engelund and Hansen [1967]

eliminated an excess shear stress term by setting the critical shear stress equal to 0.06 (from the original Shields diagram) and adjusting the exponent of the  $\tau^*$  accordingly:

$$i_{b_x} = 0.05 \rho_s v_x^2 \sqrt{\frac{d_{50_x}}{g \left( \frac{\rho_s}{\rho} - 1 \right)}} (\tau_x^*)^{1.5} \quad (5)$$

where  $i_{b_x}$  is the unit bedload transport rate in kg/s per m of width,  $\rho_s$  is density of sediment (assumed to be 2650 kg/m<sup>3</sup>), and  $d_{50}$  is the median grain size (m) of a particular size class. (Equation (5) is a correction of Equation 2.234e, [Vanoni, 1975] for dimensional homogeneity). Again the subscript  $x$  denotes computations for the cross section as a whole.

It is undesirable to have  $\tau_c^*$  hard-wired into the equation and I have thus used the original (uncalibrated) equation (not in [Vanoni, 1975]), which contains an excess shear stress term, for which I can specify the critical shear stress. I have thus revived the original equation and modified it to predict transport by grain size class and in distinct portions of the cross section:

$$i_{b_{ip}} = \alpha \left( \frac{\rho_s v_p^2 d_{50_i} (\tau_p^* - \tau_c^*)^{1.5}}{2 \sqrt{g h_p s_x}} \right) \quad (6)$$

where  $i_{bip}$  is the unit bedload transport rate in kg/s per m of width of size class  $i$  in portion  $p$  of the cross section,  $\tau_x^*$  is the Shields number computed for  $h_x$  and  $d_{50x}$ ,  $\tau_c^*$  is the dimensionless critical shear stress for the whole mixture, and  $\alpha$  is a fitting parameter. Note there are other difference between (5) and (6) which result from differences in derivation. However, each is dimensionally homogenous. The modified equation ensures that transport will only be predicted if shear stress exceeds the threshold value. I calibrated (6) to bedload datasets collected in the Sacramento River and other fluvial environments.

I fitted the  $\alpha$  parameter to bedload data in various grain size classes for each cross section with bedload data. The parameter was adjusted to achieve the best fit between computed and measured bedload for transport rates greater than 100 kg/s. Figure 3.4 shows the power of (5) and (6) to predict fractional sediment transport for bedload data from the Clearwater River in Idaho. The figure shows the original (unmodified) Engelund-Hansen equation (a) and my modified and calibrated version of the equation (b). Clearly there is an improvement in prediction with the modified, calibrated equation. The original equation fails to predict transport rates within a factor of two for most of the data. This is probably due to the fact that the original equation was not designed for fractional transport, but for total loads that include multiple grain sizes. My modifications allow for adjustment of transport in each grain size class, and a variable critical shear stress.

High flux rates of bedload are the main concern because of the general experience that the majority of a river's sediment is transported by a few high flows [Lustig, 1965; Stewart and LaMarche, 1967; Pitlick, 1988]. They represent a lower limit of transport events that overwhelm the capacity of a bedload sampling device. My stochastic flow model, HYDROCARLO, was designed to simulate flow above a flood threshold [Singer and Dunne, Submitted], in order to model the effect of large events on, among other things, bedload flux. Therefore I calibrated my modified equation only to total transport rates greater than 100 t/d. This will improve the prediction of sediment transport during the highest flood peaks and my overall estimation of long-term bedload flux.

In the calibrations of the modified Engelund-Hansen equation (6), I sought to develop a calibrated equation that could be applied to predict sediment transport of any grain size class and at any cross section within the Sacramento basin. However, ample mainstem bedload data (e.g. at least 10 measurements) for calibration were limited to two gauging stations (Bend Bridge and Hamilton City, Figure 3.1) and included only the finer grain sizes present in the bed material. Therefore, I calibrated my modified equation for each grain size class (i.e. including all fractions present in the bed material, but not significantly represented in suspended samples, Figure 3.3) using data from other fluvial environments. In addition to the aforementioned Sacramento data, I used Helley-Smith bedload data from Clearwater and Snake Rivers in Idaho and the Tanana River in Alaska, which were publicly available [Emmett and Seitz, 1973; Emmett and Seitz, 1974; Jones and Seitz, 1979; Jones and

Seitz, 1980; Burrows et al., 1981; Harrold and Burrows, 1983]. Figure 3.5 shows my fitted  $\alpha$  values plotted against grain size for five datasets, including the two from the Sacramento River.

It is apparent from this plot that fitted alpha values show a relationship with grain size. It also appears that the curves are superposed. I analyzed fitted alpha values for the various datasets and determined that superposition of the alpha curves can be explained as a function of both grain size and bed material sorting. Sorting is sedimentology parlance for the "spread" or standard deviation of a grain size distribution. The sorting coefficient of the bed material, first presented by [Krumbein, 1938], describes the sorting of the bed. High values of sorting coefficient signify a large standard deviation and vice versa. I computed sorting coefficient (phi scale) by the method of moments within GRADISTAT, a grain size analysis software [Blott and Pye, 2001].

I computed alpha in a multiple regression model as a function of grain size and bed-material sorting (adjusted  $R^2 = 0.86$ ):

$$\log_{10} \alpha = 1.95 * \sigma_{\phi} - 0.420 * \log_2 d_{50_i} - 4.664 \quad (7)$$

where  $\sigma_{\phi}$  is sorting coefficient of the bed material (phi scale). I tested model assumptions by assessing the normality and randomness of the standardized residuals.

This relationship probably emerges because poorly sorted beds have lower pocket angles leading to lower critical shear stresses and higher sediment transport

rates [Wilcock, 1998]. I use (7) to determine alpha for cross sections with no bedload data (only bed-material grain size data) and to extend alpha for larger grain sizes because Sacramento bedload data are limited to sizes less than 16 mm.

## **Daily Bedload Flux Simulation and Total Load Evaluation**

To summarize my method, I ran HEC-RAS driven by fifty, 30-year HYDROCARLO streamflow simulations and use the stage output with (1), (2), (3), (4), and (6) to obtain daily sediment transport estimates for each grain size class in each portion of a cross section. I compute bed-material flux for each grain size class multiplied by its percentage in the bed material (excluding surface armor).

For simplicity, I also assumed one-dimensional flow, no armoring of the bed surface, and no cross-sectional change, all of which could be relaxed in later iterations of the model. Beyond the percentages of each grain size class present in the bed material, I place no limits on sediment supply as transport rates increase (e.g. armoring, scour depth) in the current version of this method. Armoring of the river bed due to selective transport of small grain sizes increases the median grain size and increases sorting (decreases the sorting coefficient, or standard deviation of grain sizes), resulting in less sediment transport. Scour of bed sediments during flood events generally only occurs down to a depth limited by local geology and grain sizes at this depth. Therefore, sediment transport during a flood event can only occur until the scour depth is reached, at which point it would shut off. Although these effects are clearly important in order to obtain accurate estimates of bed-material transport,

there are currently no data for assessing their influence in the Sacramento. Consequently, I have not as yet incorporated armoring and scour depth into this version of the modeling method. However, this study is concerned with modeling spatial patterns in sediment storage, which may be computed to first order with the current method. As such, the estimates of bed-material transport and storage presented here are meant to generate an understanding of spatial patterns of sediment transport through a large river system and should not be used for any design purpose. I have a plan to systematically assess Sacramento River bed-material and scour depths in future work. This will enable me to adapt the method to account for armoring and limits on scour.

I computed daily bed-material loads for the entire cross section in each size class for each simulation as:

$$i_{bD_{ix}} = \sum_p i_{b_{ip}} w_p \quad (8)$$

where  $i_{bD_{ij}}$  is daily ( $D$ ) bed-material transport and  $w_p$  is the width of a particular portion of the cross section. Next, I computed long-term average sediment load for each simulation:

$$i_{bY_{ix}} = \frac{\sum i_{bD_{ix}}}{t} \quad (9)$$

where  $i_{bY_{ix}}$  is annual (Y) total bed-material load and  $t$  is the number of years in each simulation. And finally, I calculated the annual transport extrema (i.e. maximum and minimum) and median for all simulations. Thus, my method results in estimates of central tendency, as well as variability in transport prediction (based on stochastic hydrology).

It is important to distinguish my method from one that seeks to characterize measurement or modeling uncertainty (e.g. [Wilcock, 2001]). My method uses the variability in the flow regime to define the range and probability distribution of sediment flux as to be expected from the variable flow (and ultimately precipitation). I have minimized the uncertainty in hydrology by modeling it [Singer and Dunne, Submitted]. If one were trying to make a single estimate of long-term sediment flux, my method provides additional estimates of the range around that long-term value. I obtain these additional estimates by statistically analyzing the results of multiple long-term simulations of stochastic hydrology. The error bars around an estimate, therefore, are not estimates of uncertainty; they are estimates of variability due to flow.

Figure 3.6 shows annual total bed-material load in tons/year plotted against exceedence probability for gravel and sand at one mainstem station (Hamilton City,

Figure 3.1). This figure combines simulated bed-material loads for gravel and sand grain sizes into sand and gravel classes, respectively, for simplicity of illustration. Each simulation produces a set of dots, one for each exceedence probability. Each set of thirty dots can be thought of as a sediment load frequency curve, akin to a flood frequency curve. The solid line represents the median value of all simulations and the dashed lines represent the extrema. For example, my simulations show that in about 50% of years annual total gravel transport at Hamilton City exceeds a value that ranges from ~20-400 kt/y with a median of ~200 kt/y. For resolution of this calculation, a reach width of 200 m, an upstream recruitment distance of 800 m (average annual transport distance of gravel tracers in [*California Department of Water Resources*, 1992] is within a range suggested by [*Bunte and MacDonald*, 1999]), and a sediment bulk density of  $1.8 \text{ t/m}^3$ , the computed annual sediment load at Hamilton City would scour to a depth of ~0.7 m. Although this calculation does not reflect process of scour and fill that may prevail over a year, it does illustrate the need to account for scour depth and armoring in future iterations of this method.

In the following paragraphs I present transport results for each mainstem gauging station based on these simulations. In the subsequent section, I use these transport estimates and those from tributaries to evaluate net changes in storage in the reaches of river between each mainstem gauging station. I assume that net changes in storage are spread evenly throughout a river reach.

Figure 3.7 shows the results of gravel and sand bed-material transport for my simulations at all mainstem cross sections. I have also plotted suspended load

simulated in my previous analysis [*Singer and Dunne, 2001*] and total load obtained by summing sand, gravel, and suspended loads. The method predicts that gravel transport makes up anywhere from 0-33% of the total load depending on the station, which is an expectable range.

A few noteworthy general results about local transport emerge from the modeling. Most importantly, local hydraulics and bed-material grain size distributions conspire to control annual transport rates at a given cross section. The effect of hydraulics on transport rates at mainstem stations is apparent in that downstream changes in annual load correlate with changes in local water surface slope (Figure 3.7 and Table 1). Bed grain sizes influence transport patterns in two ways. First, at locations where bed sediments are well sorted (e.g. Sacramento (SA), Table 3.1), transport rates are low (Figure 3.7), and at locations where there is high variance in bed grain sizes (e.g. Knights Landing (KL), Table 3.1), transport rates are high (Figure 3.7). Second, the percentage of a particular grain size in the bed at a cross section controls its transport relative to other size classes. For example, gravel bed-material load is slightly higher than sand bed-material load at Bend Bridge (BB) due to a relative scarcity of sand in the bed (17% sand > 0.5 mm). Although both of these conclusions are consequences of modeling assumptions, they appear to reflect empiricism. In fact, the high value of  $R^2$  (0.86) for the multiple regression model (7) used to estimate the alpha parameter in (6) indicates the large influence that bed-material grain sizes have on bedload transport rates for various datasets.

The presented method produces transport patterns similar to those obtained for suspended sediment transport modeling by empiricism, suggesting that the method is capable of reproducing empirical patterns in bed-material transport. For example, both transport studies predict an increase in transport between Hamilton City (HC) and Butte City (BC), which was explained for suspended load by the influence of flood control levees in Reach 2 [*Singer and Dunne, 2001*]. It appears that the predicted increase in bed-material transport is, at least in part, due to a decrease in coarse sediments and an increase of medium sand in the bed material at BC (Figure 3.3). This change in bed material probably arises because the Sacramento River downstream of HC has no contiguous contact with Pleistocene river gravels (Red Bluff formation in 1:250,000 Calif. Division of Mines and Geol. quadrangles). My method also predicts a decrease in bed-material load between Butte City (BC) and Colusa (CO), which is consistent with the dramatic reduction in suspended sediment load simulated in a previous study [*Singer and Dunne, 2001*]. Colusa signifies a transition in transport pattern, where a major deflection of the river eastward around the Colusa Dome, the result of a magmatic intrusion 1.4-2.4 Mya and localized movement on the Willows fault [*Harwood and Helley, 1987*], appears to force decanting of washload into upstream flood bypasses [*Singer and Dunne, 2001*] and systematic deposition of sediments in the wide upstream reach of valley.

In other locations, predicted bed-material transport patterns diverge from their suspended load counterparts. This method predicts a decrease in bed-material transport between BB and HC (Figure 3.7), which probably reflects the increase in

valley width associated with the Sacramento's transition from an entrenched river in Iron Canyon to an aggraded, lowland river in the Central Valley. The valley width increase allows for more in-channel accommodation space, where bed sediments can organize into defined bedforms, perhaps resulting in better sorting of the bed-material mixture (i.e. lower sorting coefficient). Bed-material calculations also show an increase in bed-material load between CO and KL (Figure 3.7), which is consistent with the observation of an abrupt increase in 8-32 mm gravels and medium sand in the bed material at Knights Landing (Figure 3.3). These factors suggest that there is a sediment source in Reach 4. Inspection of the Sacramento geologic quadrangle (1:250,000, Calif. Div. of Mines and Geol.) reveals that the Sacramento River is dissecting Pleistocene fanglomerates of Cache Creek, which extend across the floodplain in Reach 4. The local change in bed-material results in a relatively high sorting coefficient (Table 3.1) and thus, high bed-material transport. Finally, bed-material calculations predict huge declines in transport between KL and Sacramento (SA). This result stems from an extremely low sorting coefficient at SA (Table 3.1), minute quantities of gravel in the bed material (Figure 3.3f), and low (or occasionally negative) water surface slopes at this section, which is located in the tidal zone. These factors do not, however, appear to influence suspended load, which increases at Sacramento probably because of fine sediment delivery from Feather and American Rivers (tributaries shown in Figure 3.1).

The method presented here can also be used to simulate annual peaks in bed-material load to ascertain the role of individual flood events on sediment transport. I

computed annual peak bed-material load as the one-day maximum load for each year. As before median and extrema of this value, for a given exceedence probability, are determined for the 50 simulations. Figure 3.8 shows one-day peak bed-material load for sand and gravel. The highest one-day sand transport peak for all simulations is ~340 kt, or ~170% of the median annual total sand flux at Hamilton City. Annual totals and one-day peaks of bed-material transport will be used in the next section to evaluate net changes in reach-averaged sediment storage.

## **Bed-material Budgets**

I evaluated simple mainstem sediment budgets from the estimates of total annual bed-material load and one-day maximum bed-material load into the Sacramento from tributaries and past each mainstem gauging station. These are crude mass balances in the sense that I compute how much sediment gets stored in or eroded from a given reach, but I provide no mechanistic explanation of how the mass balance is being struck within the reach (e.g. changes in morphology). For simplicity, I assume that simulated erosion for a reach is distributed uniformly over the bed surface, in order to compute reach-averaged erosion rates.

I computed bed-material influx to the Sacramento River from four signature tributaries, which represent the four geologic provinces used in *Singer and Dunne* [2001]. Tributary loads were also computed by driving (6) with discharge data simulated by HYDROCARLO [*Singer and Dunne*, 2001]. However, instead of routing this flow with HEC-RAS, I obtained mean flow depths,  $h_x$ , for each day from

stage-discharge rating curves. Since I had no calibrated values of Manning's  $n$  to compute velocity in (2), I used a velocity-stage rating curve from USGS field measurements. And I measured slopes from USGS 7.5-minute topographic quadrangles for use in (3). As in the suspended load study, I scaled the computed signature tributary loads (and their uncertainties) by the ratio of drainage areas to compute the load entering the mainstem from each Sacramento tributary. I combined these time varying loads with those computed for mainstem stations to evaluate simple, reach-averaged, bed-material budgets.

### **Annual Total Bed-material Load**

I computed simple budgets for annual total bed-material load, which indicates long-term spatial patterns in mainstem sediment transport. Annual divergence, or net difference in bed-material load, was computed for each reach as:

$$\Delta i_{bYR} = i_{bYU} - i_{bYE} + i_{bYL} \quad (10)$$

where  $\Delta i_{bYR}$  is reach-averaged ( $R$ ) change in annual ( $Y$ ) total bed-material load;  $i_{bYU}$  is annual total bed-material load entering the reach from upstream ( $U$ );  $i_{bYE}$  is annual total bed-material load leaving the reach at its downstream end ( $E$  for efflux); and  $i_{bYL}$  is the annual bed-material load entering the reach from tributaries ( $L$  for lateral input). I assume that no bed-material load leaves the reach through flood diversions, which decant mostly washload [*Singer and Dunne, 2001*], and that fining by attrition is

negligible. This type of budget may be computed for each grain size (because I compute fractional transport rates), but for simplicity I present results from budgets computed for total bed material load (a), gravel load (b), and sand load (c) (Figure 3.9). The computational spreadsheets for annual gravel and sand bed-material load are contained in Appendix C and D.

The bars in Figure 3.9 represent the median of the expected range (i.e. the 50% exceedence probability) of net erosion or deposition for a year and for a reach, and the T-bars represent the extrema of this range resulting from all simulations of stochastic hydrology (i.e. fifty 30-year runs). The T-bars increase in magnitude in the downstream direction because I propagated the variability. The upper T-bars, for example, represent the maximum of the expected range (i.e. the 50% exceedence probability) for all upstream mainstem stations and tributaries added together. The lower T-bars represent the same for the minimum of the range.

The budget for annual total bed-material load indicates significant net bed-material erosion in Reaches 0, 2, and 4, and deposition in Reaches 1, 3, and 5 (Figure 3.1). I compared this budget with one previously evaluated for suspended load (Figure 6 in [*Singer and Dunne, 2001*]), which identified erosion in Reaches 2, 4, and 5 and net deposition in Reaches 0, 1, and 3. Reaches 1, 2, 3, and 4 show a similar pattern in both budgets, indicating there are potentially similarities in storage patterns between the various modes of sediment transport. It should be noted that the suspended load budget was evaluated using historical flow, because the time series approach used in that study does not lend itself to simulation under a range of flow

conditions. An explanation of the differences between the bed-material load and suspended load budgets requires a better understanding of the sources of and the controls on washload in the Sacramento basin, so the following discussion will be limited to the simulated bed-material budgets.

Figures 3.9b and 3.9c show annual total budgets for gravel and sand, respectively. These budgets are subsets of Figure 3.9a that reveal which grain size fractions are responsible for the net divergence in a given reach. The majority of the simulated divergences result from imbalances in sand bed-material transport, as one would expect. However, significant gravel divergences can indicate the state of the riverbed in a given reach.

For example, gravel erosion is predicted in Reaches 0, 2, and 4. Annual gravel erosion in Reach 0 is predicted to be 7 cm/y when averaged over the area of the bed in that reach (assuming sediment density of  $1.8 \text{ t/m}^3$  and transporting width of 150 m). With no additional upstream sources of gravel entering the reach (i.e. beyond the simulated tributary input), net erosion in this reach is predicted to prevail. Annual gravel erosion rates in Reaches 2 and 4 are predicted to be 5 cm/y and 15 cm/y, respectively. Perhaps most interesting is the high gravel erosion rate predicted in Reach 4. As previously discussed, this erosion likely results from the dissection of a Pleistocene fan composed of fine and medium size gravels. An increase in gravel transport seems reasonable in a locale where a local source of gravel can be transported over an increasingly sandy bed (Figure 3.3). It is not reasonable, however, to expect that predicted erosion in any river reach would be spatially

uniform. The method presented here can resolve transport rates for each portion of a cross section, but no such assessments can be made of river reaches. I have a plan to conduct high-resolution sediment routing through each reach to determine where topographic adjustments within a river reach might be expected.

Significant sand erosion is predicted in Reaches 2 and 4, but is highest in Reach 4. The erosion of sand predicted in this reach is in part, due to a shift in grain sizes in suspension. For reasons that are not clear, Figures 3.3d and e show the suspended load fines between CO and KL. For example, the 0.38 mm fraction decreases from 7% to 2.5% of the suspended load, with no apparent change in its presence in the bed material. Consequently, I included the 0.38 mm size fraction in my computations of bed-material load, and this, alone, may account for the high erosion of sand bed-material predicted in Reach 4.

The deposition in Reach 3 probably results from water sequestration above Colusa as previously discussed. Deposition in Reach 5 is the combined effect of large sand loads into this reach from the Feather River and significant fine gravel loads entering from upstream. It appears that Reach 5 is a sink for gravel. Based on recent floodplain cores we have extracted from Yolo Bypass (unpublished data), it is likely that a large percentage of the sand bed material (e.g. the fine fractions) being deposited in this reach actually passes over Fremont Weir into Yolo Bypass (Figure 3.1), which shunts flood flow from the Sacramento River.

### **One-day Peak Bed-material Load**

I computed a simple budget for one-day annual peak bed-material load, which indicates the spatial effects of maximum flux into and through the mainstem Sacramento. I simulated peak sediment delivery to the Sacramento from tributaries and past mainstem gauging points. This calculation indicates the short-term consequences of scour and fill in large floods. The peak budget is computed as:

$$\Delta i_{bD_{\max}R} = i_{bD_{\max}U} - i_{bD_{\max}E} + i_{bD_{\max}L} \quad (11)$$

where the symbols are the same as in (10), but the subscript  $D_{\max}$  refers to one-day annual peak bed-material load. Figure 3.10 shows the results of this budget, where the symbols are the same as in Figure 3.9. The computational spreadsheets for peak gravel and sand bed-material load are contained in Appendix E and F. The spatial patterns for this budget are similar to those of the annual total budget. Erosion is predicted in Reaches 0, 2, and 4 and deposition prevails in Reaches 0, 3, and 5. In other words, the total annual budget is an integration of flood conditions that induce similar patterns in net bed-material load divergence.

## Discussion

I have developed a method for simulating daily bed material flux, but it cannot yet be tested empirically, because such data do not exist. To reduce sources of uncertainty not associated with stochastic hydrology, I have tried to accurately parameterize each equation based on the best available datasets of channel

dimensions and hydraulic data, bed material texture, and bedload transport. The accuracy of transport predictions (and budgets) can be improved for a particular basin by collecting more field data. I have already discussed the need for assessing armoring and scour depth, but there are other data collection opportunities that would improve this method. For example, simulations on the Sacramento would benefit from bedload measurements and bed material surveys for each major tributary to simulate influx from each separately, instead of scaling loads from signature tributaries. Additional cross sections could also be surveyed in tributary basins so that explicit flood routing could be conducted to obtain water surface profiles for use in (2), and to calibrate Manning's  $n$  for use in (3). Bedload flux measurements for Knights Landing, Sacramento, Feather River, and other sandy environments would also be useful to determine  $\tau_c^*$  for these stations and to improve transport calibrations for sand-bed rivers. More bed material samples are required to accurately characterize grain size distributions at all stations, especially Bend Bridge and Hamilton City where these data are limited.

The method introduced here simulates sediment flux associated with flood days above a threshold. This threshold was developed by a repeatable statistical procedure [*Singer and Dunne*, Submitted], without consideration of thresholds for sediment transport, for instance. This is because HYDROCARLO was designed to simulate flows at the upper, less frequent end of the flood frequency curve. I assume that these floods do most of the geomorphic 'work' (i.e. sediment transport) in sediment transport [*Lustig*, 1965; *Stewart and LaMarche*, 1967; *Pitlick*, 1988].

I tested the assumption that flood events transport the majority of sediment in the Sacramento basin. I computed bed material sediment load for non-floods by driving equations (1), (2), (3), (4), and (6) with the threshold flood condition for each station. I multiplied the geometric mean of baseline transport (i.e. square root of the computed bed-material transport at the flood threshold) by 365 days to assess annual transport rates during non-floods. Consistent with other findings on California rivers [Lustig, 1965; Stewart and LaMarche, 1967; Pitlick, 1988], sediment transport in the Sacramento River is dominated by floods. According to my analysis, flood days are anywhere from 17 to 64 times more effective than non-flood days at transporting bed-material in the Sacramento River. Floods dominate geomorphic work in the Sacramento basin, though it is a subject of further research to determine which floods (e.g. large, infrequent or small, frequent) do the majority of the geomorphic work [Wolman and Miller, 1960; Wolman and Gerson, 1978].

I have demonstrated how my method of basinwide sediment flux simulation may be applied to sediment budgets, but it may also be useful in predicting channel geometry resulting from an integration of rare, large flows over a period of years or decades. It has further potential to aid in the design and implementation of river rehabilitation strategies (e.g. gravel augmentation), which generally require a prediction horizon of decades and a characterization of risk.

## **Conclusion**

I have developed and demonstrated a method for simulating basinwide bed-material flux and storage change based on variability in flow. I applied the model to the Sacramento River basin to simulate daily influx to and through the mainstem Sacramento. The model may be used to estimate the central tendency and extrema of annual total and one-day peak flux. These estimates can then be used in work on sediment budgets, channel morphology, and river rehabilitation. Simulations in the Sacramento basin highlight imbalances in bed-material transport and storage that, in a general way, point to local hydraulics and downstream changes in grain sizes in the riverbed. They also confirm the assumption that floods transport the majority of bed-material in the Sacramento River.

## References

- Andrews, E.D., Measurement and computation of bed-material discharge in a shallow sand-bed stream, Muddy Creek, Wyoming, *Water Resources Research*, 17 (1), 131-141, 1981.
- Ashida, K., and M. Michiue, Study on hydraulic resistance and bedload transport rate in alluvial streams, *Transactions, Japan Society of Civil Eng.*, 206, 59-69, 1972.
- Batalla, R.J., Evaluating bed-material transport equations using field measurements in a sandy gravel-bed stream, Arbucies River, NE Spain, *Earth Surface Processes and Landforms*, 22, 121-130, 1997.
- Blott, S.J., and K. Pye, Gradistat: A grain size distribution and statistics package for the analysis of unconsolidated grains, *Earth Surface Processes & Landforms*, 26, 1237-1248, 2001.
- Buffington, J.M., and D.R. Montgomery, A systematic analysis of eight decades of incipient motion studies with special reference to gravel-bedded rivers, *Water Resources Research*, 33 (8), 1993-2029, 1997.
- Bunte, K., and L. MacDonald, Scale considerations and the detectability of sedimentary cumulative watershed effects, pp. 328, National Council for Air and Stream Improvement, Technical Bull. 776, Research Triangle Park, NC, 1999.
- Burrows, R.L., W.W. Emmett, and B. Parks, Sediment transport in the Tanana River near Fairbanks, Alaska, 1977-79, pp. 56, US Geological Survey Water Resources Investigation Report 81-20, 1981.
- California Department of Water Resources, Sacramento River spawning gravel restoration phase I progress report, pp. 37, Red Bluff, 1992.
- California Dept. of Water Resources, Sacramento River bank erosion investigation, Dept. Water Resources, Sacramento, CA, 1994.
- Dunne, T., L. Mertes, R. Meade, and J. Richey, Exchanges of sediment between the flood plain and channel of the Amazon River in Brazil., *Geol. Soc. Amer. Bulletin*, 110 (4), 450-467, 1998.
- Edwards, T.K., and G.D. Glysson, Field methods for measurement of fluvial sediment, U.S. Geological Survey., Reston, VA, 1999.

- Emmett, W.W., A field calibration of the sediment-trapping characteristics of the Helley-Smith bedload sampler, US Geological Survey, Professional Paper 1139, Washington, D.C., 1980.
- Emmett, W.W., and H.R. Seitz, Suspended- and bedload-sediment transport in the Snake and Clearwater rivers in the vicinity of Lewiston, Idaho, March, 1972 through June, 1973, US Geological Survey Report, 1973.
- Emmett, W.W., and H.R. Seitz, Suspended- and bedload-sediment transport in the Snake and Clearwater Rivers in the vicinity of Lewiston, Idaho : July, 1973 through July, 1974, US Geological Survey Report, 1974.
- Engelund, F., and E. Hansen, A monograph on sediment transport in alluvial streams, in *Teknisk Vorlag*, pp. 63, Technical University of Denmark, Copenhagen, Denmark, 1967.
- Gomez, B., and M. Church, An assessment of bed load sediment transport formulae for gravel bed rivers, *Water Resources Research*, 25 (6), 1161-1186, 1989.
- Guy, H.P., D.B. Simons, and E.V. Richardson, Summary of alluvial channel data from flume experiments, 1956-61, US Geological Survey Professional Paper 462-I, Washington, D.C., 1966.
- Harrold, P.E., and R.L. Burrows, Sediment transport in the Tanana River near Fairbanks, Alaska, 1982, US Geological Survey Water Resources Investigation Report 83-4213, 1983.
- Harwood, D.S., and E.J. Helley, Late Cenozoic tectonism of the Sacramento Valley, California, US Geol. Survey Prof. Paper 1359, Wash., D.C., 1987.
- Helley, E.J., and W. Smith, Development and calibration of a pressure-difference bedload sampler, pp. 18, US Geological Survey, Open-File Report, Menlo Park, CA, 1971.
- Jones, M.L., and H.R. Seitz, Suspended- and bedload-sediment transport in the Snake and Clearwater rivers in the vicinity of Lewiston, Idaho, August 1976 through July 1978, pp. 87, US Geological Survey Open File Report 79-417, 1979.
- Jones, M.L., and H.R. Seitz, Sediment transport in the Snake and Clearwater Rivers in the vicinity of Lewiston, Idaho, pp. 179, US Geological Survey Open File Report 80-690, 1980.
- Krumbein, W.C., Size-frequency distributions of sediments and the normal phi curve, *J. Sedimentary Petrology*, 8, 84-90, 1938.

- Lustig, L.K., Sediment yield of the Castaic watershed, Western Los Angeles County California-A quantitative approach, pp. 23, US Geological Survey Professional Paper 422-F, Washington, DC, 1965.
- McLean, D.G., Sensitivity analysis of bedload equations, in *Proceedings Canadian Society of Civil Engineering Annual Conference*, pp. 1-15, Saskatoon, 1995.
- Milliman, J.D., and R.H. Meade, World-wide delivery of river sediment to the oceans, *J. Geology*, *91*, 1-21, 1983.
- Milliman, J.D., and J.P.M. Syvitski, Geomorphic/tectonic control of sediment discharge to the ocean: The importance of small mountainous rivers, *J. Geology*, *100*, 525-544, 1992.
- Parker, G., P.C. Klingeman, and D.G. McLean, Bedload and size distribution in paved gravel-bed streams, *ASCE, Proceedings, J. Hydraulics Div.*, *108*, 544-571, 1982.
- Pitlick, J., The response of coarse-bed rivers to large floods in California and Colorado, Dissertation thesis, Colorado State University, Fort Collins, CO, 1988.
- Reid, L.M., and T. Dunne, *Rapid Evaluation of Sediment Budgets*, 160 pp., Catena-Verlag, Cremlingen, Germany, 1996.
- Shields, A., Anwendung der aenlichkeitsmechanik und der turbulenzforschung auf die geschiebebewegung, Mitteilungen der Preussischen Versuchsanstalt fur Wasserbau und Schiffbau,, Berlin, Germany (Translated to English by W.P. Ott and J.C. van Uchelen, CalTech, Pasadena, CA), 1936.
- Singer, M.B., and T. Dunne, Identifying eroding and depositional reaches of valley by analysis of suspended-sediment transport in the Sacramento River, California, *Water Resources Research*, *37* (12), 3371-3381, 2001.
- Singer, M.B., and T. Dunne, An empirical-stochastic, event-based model for simulating inflow from a tributary network: Theoretical framework and application to the Sacramento River basin, California, Submitted.
- Stewart, J.H., and V.C. LaMarche, Erosion and deposition produced by the flood of December 1964 on Coffee Creek Trinity County, California, pp. 22, US Geological Survey Professional Paper 422-K, Washington, DC, 1967.
- Vanoni, V., *Sedimentation Engineering*, 745 pp., American Soc. Civil Eng., New York, NY, 1975.

- White, W.R., W.R. Milli, and A.D. Crabbe, Sediment transport theories: a review, *Proceedings of the Institution of Civil Eng.*, 59 (2), 265-292, 1975.
- Wilcock, P.R., Estimating local bed shear stress from velocity observations, *Water Resources Research*, 32, 3361-3366, 1996.
- Wilcock, P.R., Two-fraction model of initial sediment motion in gravel-bed rivers, *Science*, 280, 410-412, 1998.
- Wilcock, P.R., Toward a practical method for estimating sediment-transport rates in gravel-bed rivers, *Earth Surface Processes & Landforms*, 26, 1395-1408, 2001.
- Wolman, M.G., and R. Gerson, Relative time scales of time and effectiveness of climate in watershed geomorphology, *Earth Surface Processes & Landforms*, 3, 189-208, 1978.
- Wolman, M.G., and J.P. Miller, Magnitude and frequency of forces in geomorphic processes, *J. Geology*, 68, 54-74, 1960.
- Yang, C.T., and S. Wan, Comparisons of selected bed-material load formulas, *J. Hydraulic Engineering*, 117 (8), 973-989, 1991.

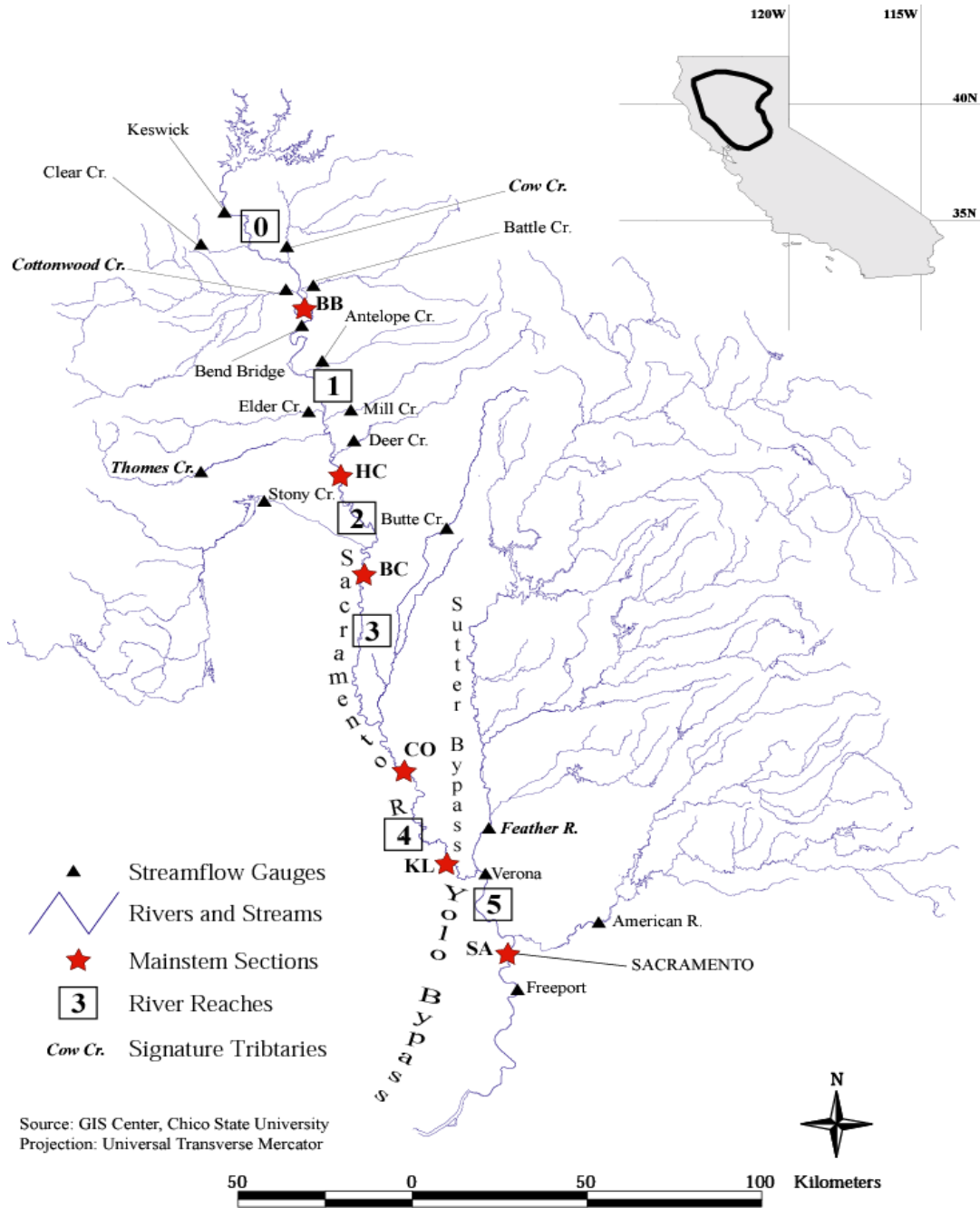


**Figure 3.1** Map of study basin showing streamflow gauges used for stochastic flow simulation, stream network, mainstem sections through which bed-material transport was computed, river reaches for which simple sediment budgets were evaluated, and signature tributaries used to compute sediment entering the mainstem from common geologic provinces (scaled by drainage area).

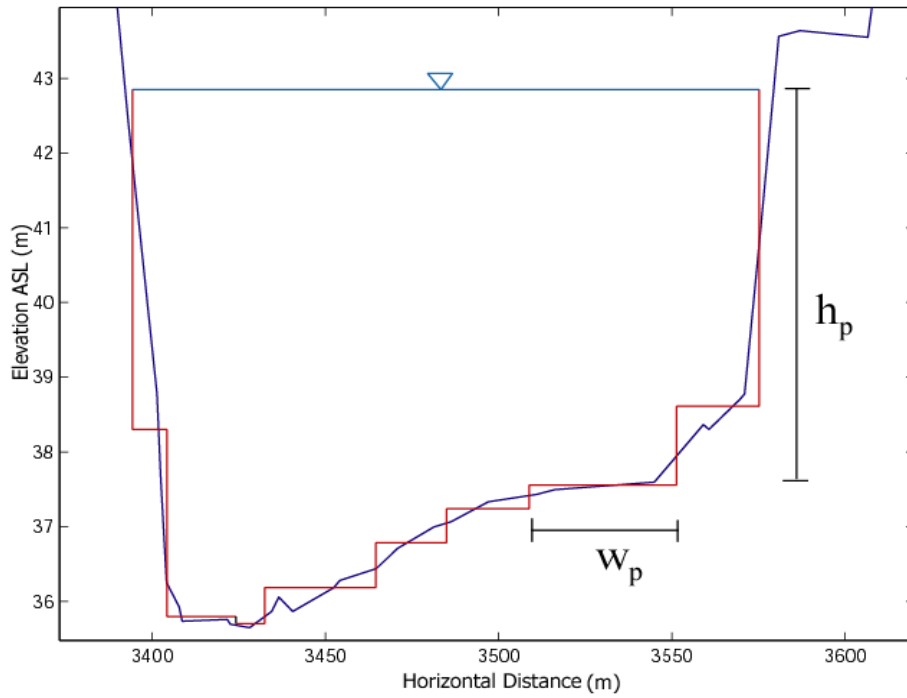


**Figure 3.2** Plot of the cross section at Hamilton City illustrating the simplification of cross sections into seven distinct portions for which I computed sediment transport. Each portion,  $p$ , has a flow depth,  $h$ , and a width,  $x$ .

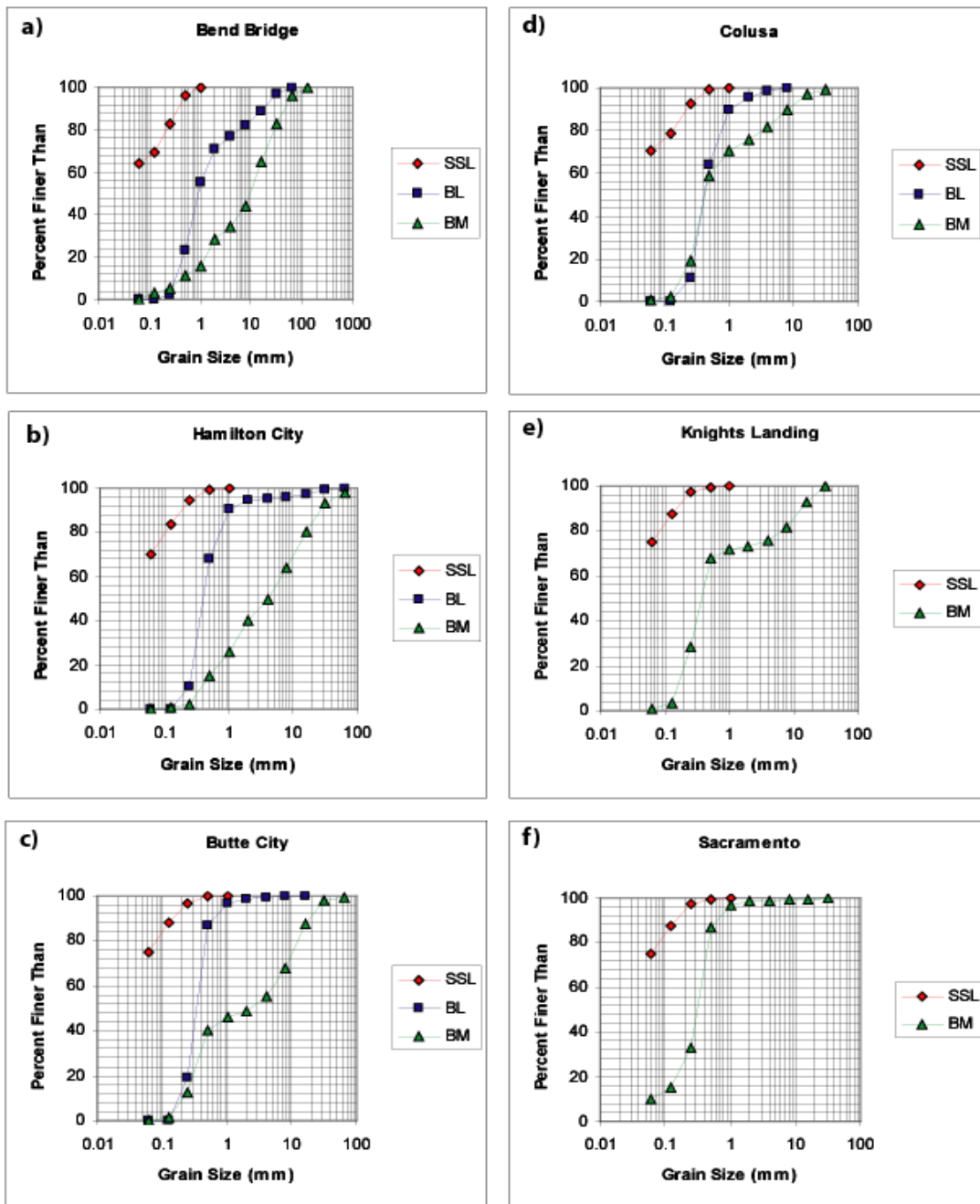


**Figure 3.3** Grain-size distributions of suspended load (SSL), bedload (BL), and bed material (BM) for the six mainstem cross sections. Generally, 0.5 mm represents a lower limit grain size of the bed material. This grain size is present in < 5% of suspended load samples and > 5% of bed material samples. Suspended load curves are generated from > 10 samples. Bedload curves are generated from between 5 and 25 samples. Bed material curves are generated from between 1 and 20 samples.

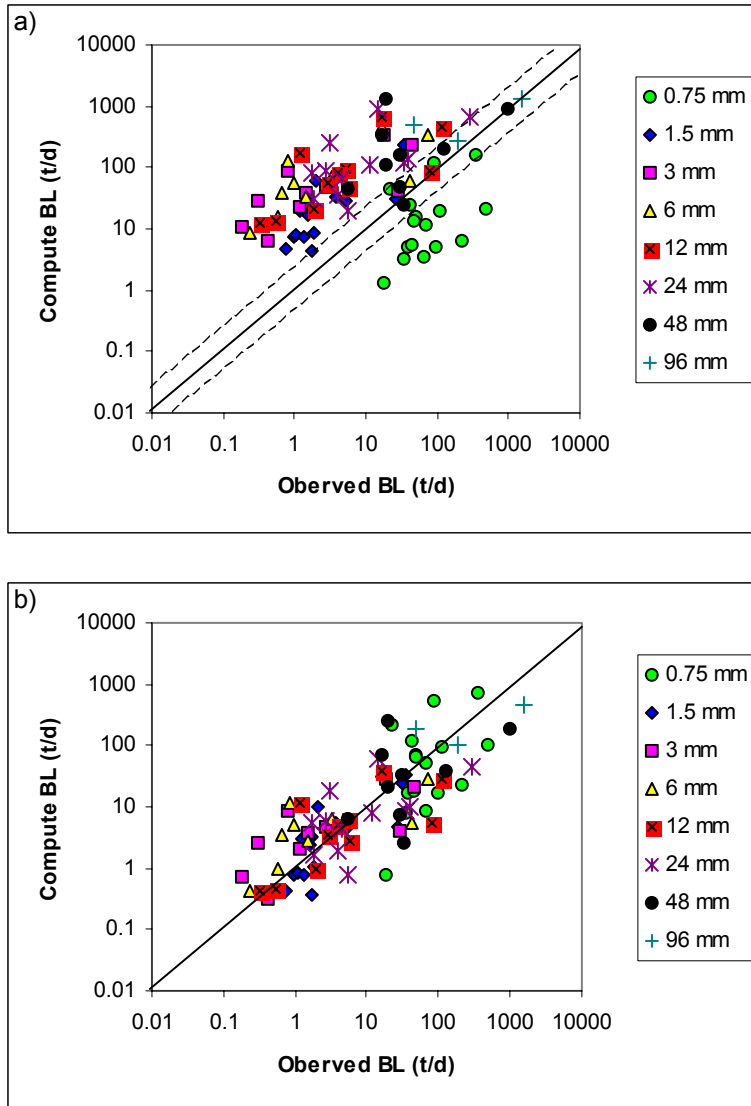


**Figure 3.4** Plots of computed bedload v. observed bedload for Clearwater River, Idaho. The different panels are a) Engelund-Hansen formula (5) predictions; b) my modified version (6) calibrated to the majority of data in each grain size class. I restricted my calibration to total transport rates (sum of all transported grain sizes) greater than 100 t/d.

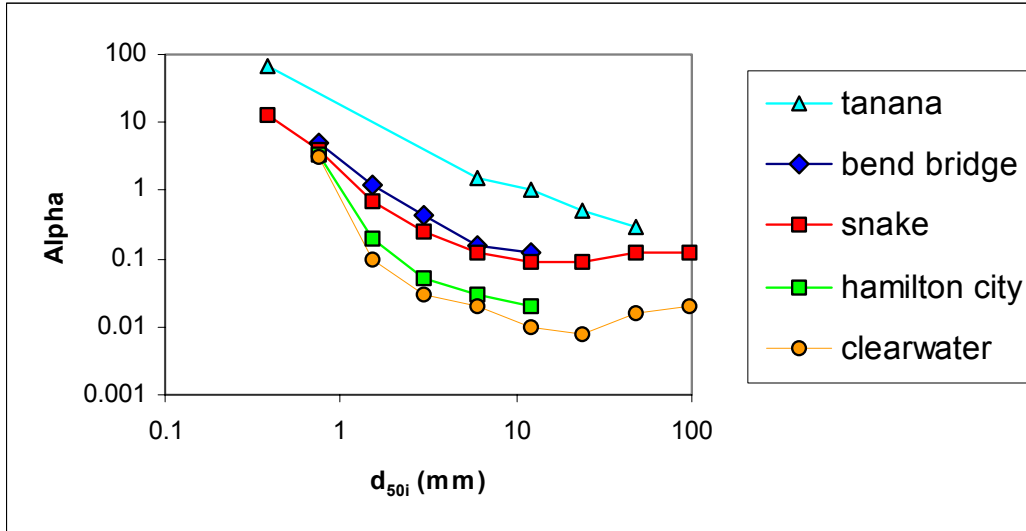


**Figure 3.5** Fitted alpha (coefficient in (6)) values from calibrations to bedload data in each grain size class. Again I restrict calibration to total transport rates greater than 100 t/d. The plot shows data from the Tanana River in Alaska, Bend Bridge and Hamilton City in the Sacramento basin, and the Snake and Clearwater Rivers in Idaho.

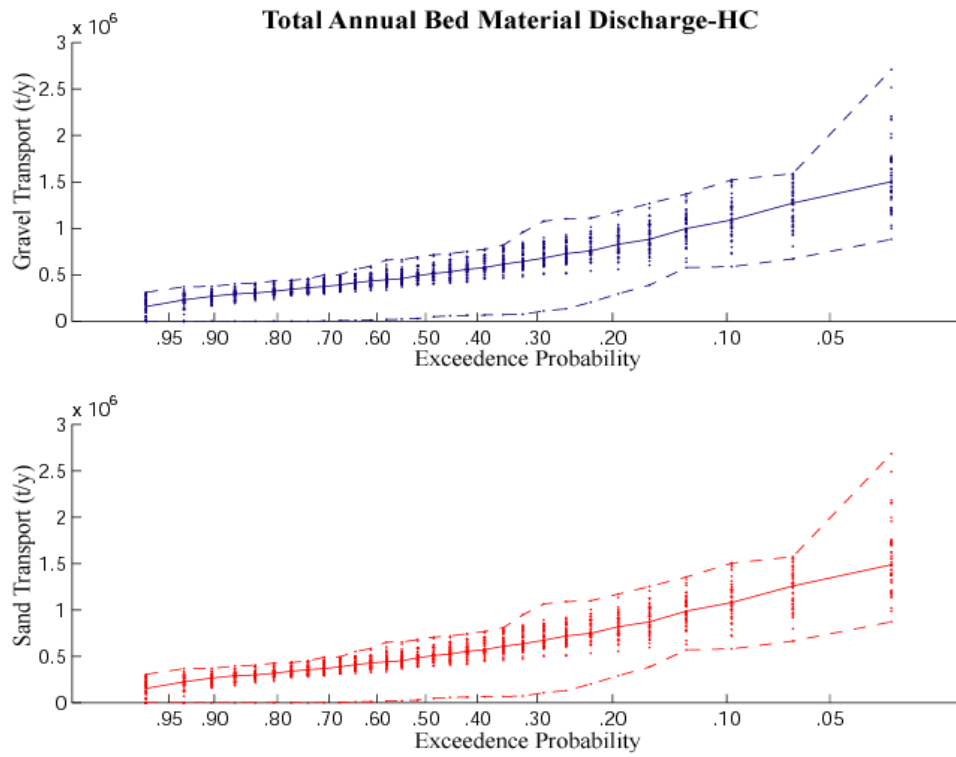


**Figure 3.6** Total annual bed-material loads (t/y) for gravel (upper panel) and sand (lower panel) at Hamilton City plotted against exceedence probability. Each simulation produces 30 dots (one for each year). The median of all simulations is represented by the solid line and the extrema by dashed lines.

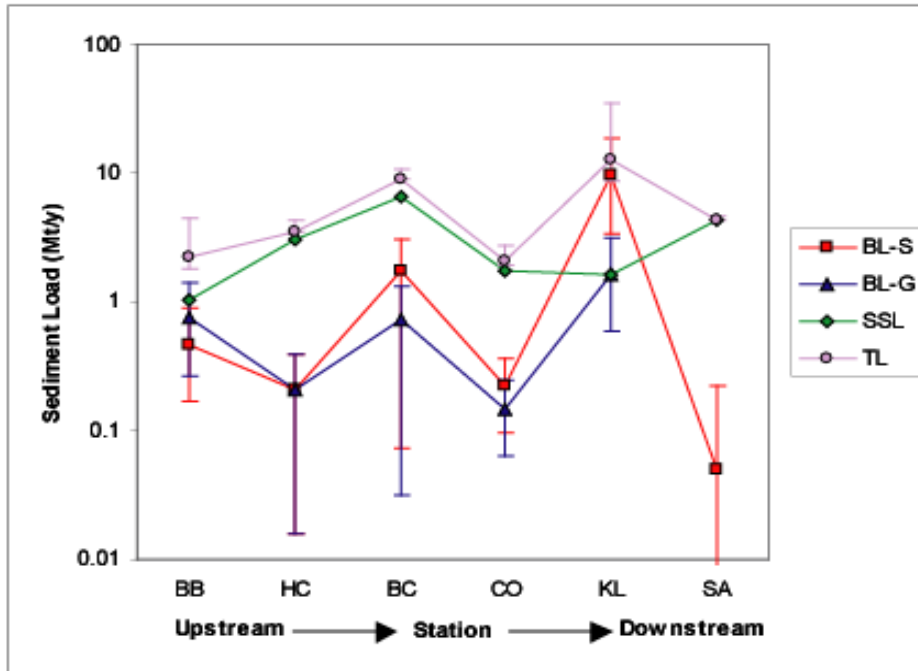


**Figure 3.7** Mainstem sediment loads (Mt/y) including total load (TL), suspended load (SSL), sand bed-material load (BL-S), and gravel bed-material load (BL-G). Suspended loads were simulated in a previous study [Singer and Dunne, 2001]. The error bars on the bed-material estimates represent the uncertainty associated with stochastic hydrology.

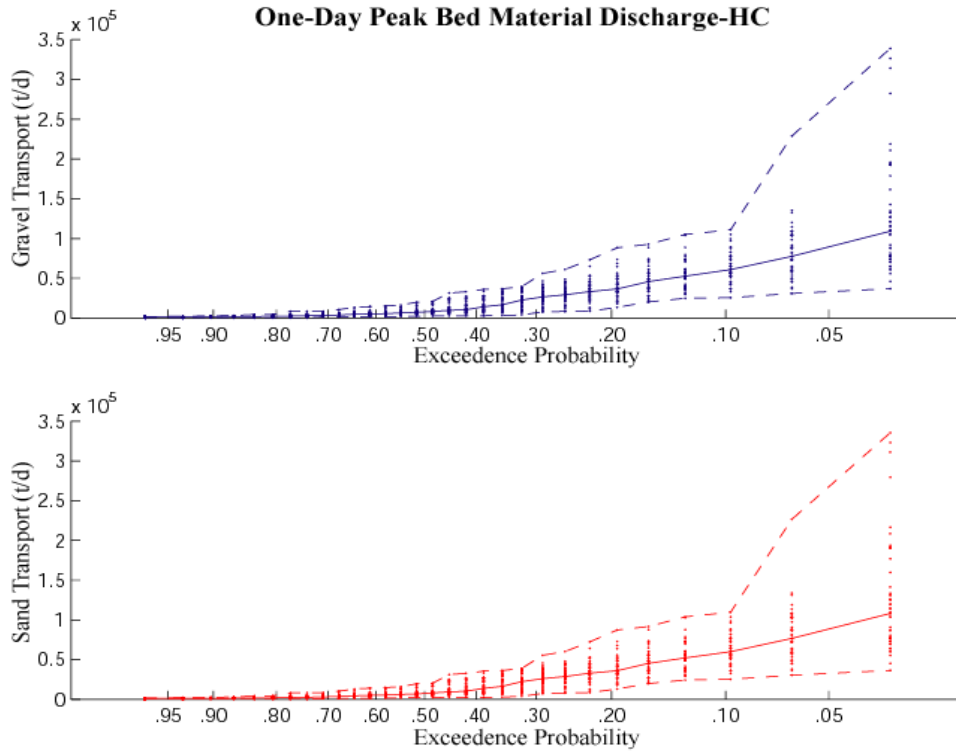


**Figure 3.8** One-day peak bed-material loads (t/d) for gravel (upper panel) and sand (lower panel) at Hamilton City plotted against exceedence probability. Each simulation produces 30 dots (one for each year). The median of all simulations is represented by the solid line and the extrema by dashed lines.

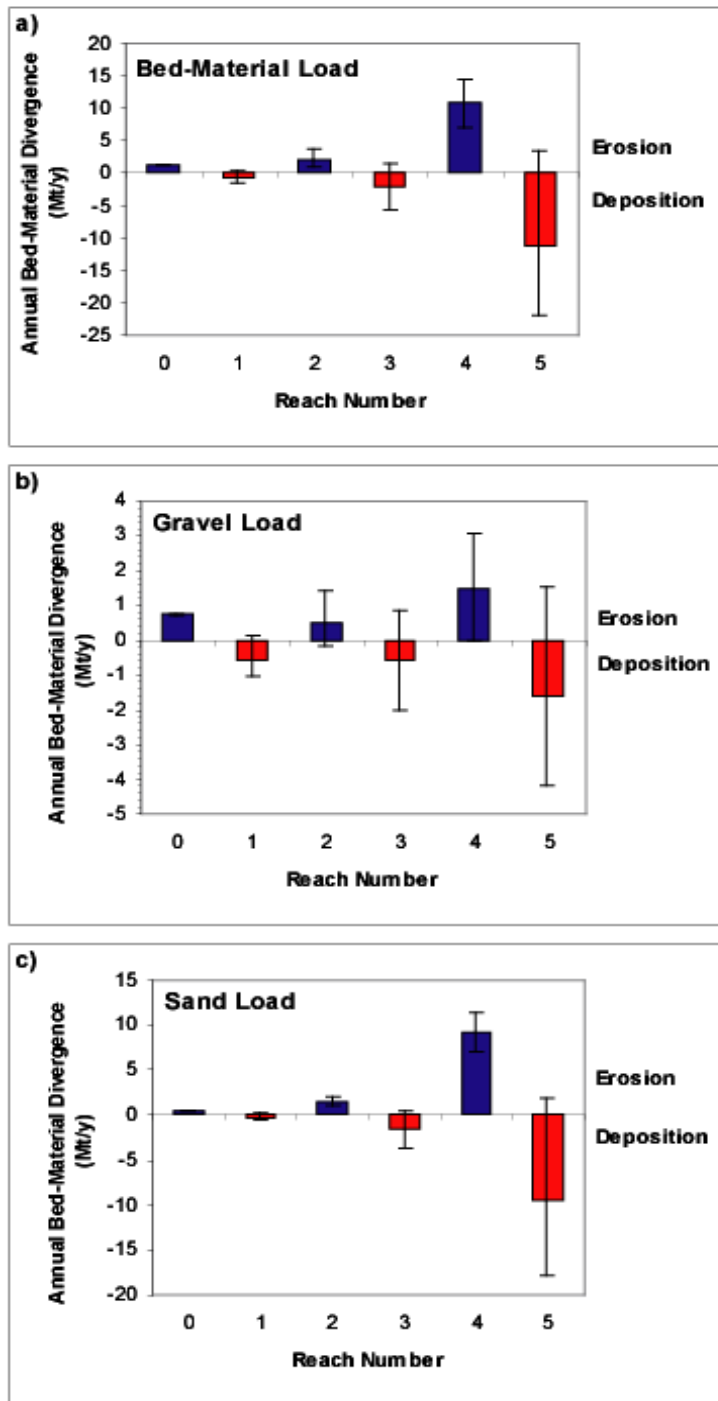


**Figure 3.9** Simple total annual bed material budgets for all bed material (a), the gravel portion (b), and the sand portion (c). Divergences (Mt/y) are net differences in sediment transport for each reach. Negative divergence is deposition and positive is erosion. Error bars represent the variability in the annual total divergences associated with stochastic hydrology, which was propagated downstream.

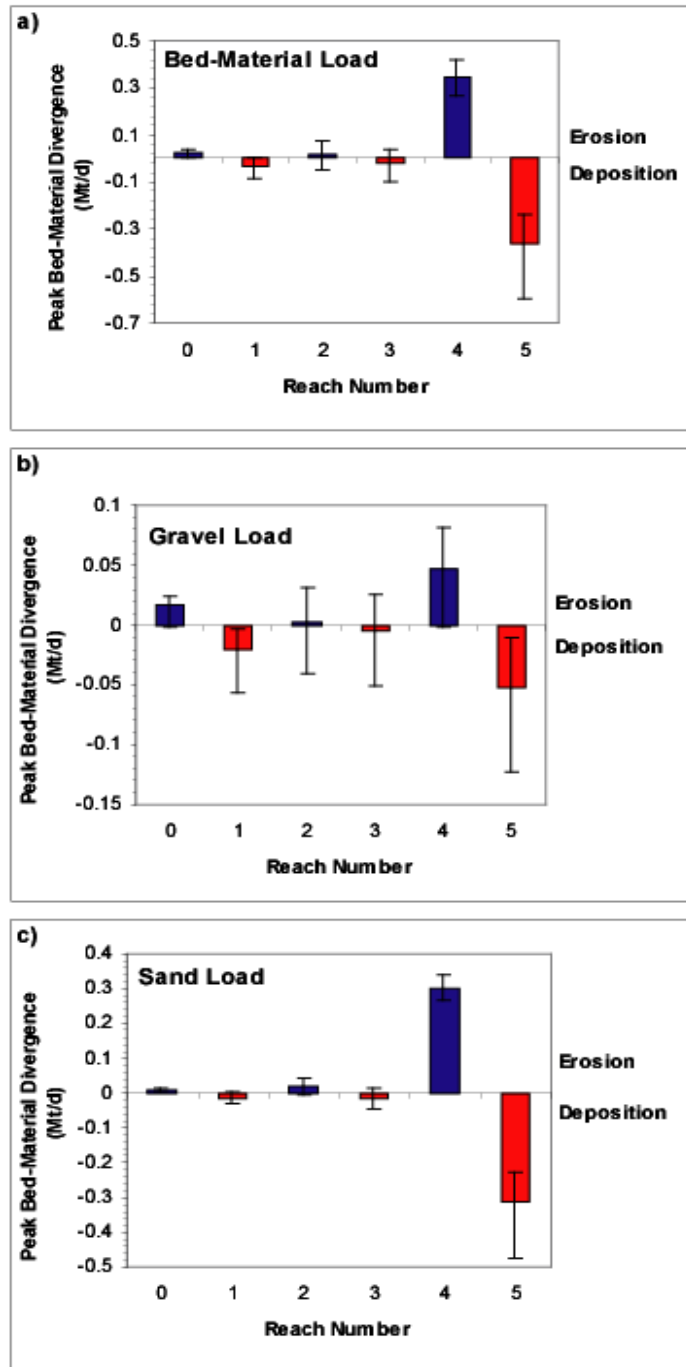


**Figure 3.10** Simple one-day peak bed material budgets for all bed material (a), the gravel portion (b), and the sand portion (c). Divergences (Mt/d) are net differences in sediment transport for each reach. Negative divergence is deposition and positive is erosion. Error bars represent the variability in the one-day peak divergences associated with stochastic hydrology, which was propagated downstream.

Station	Drainage Area (km <sup>2</sup> )	River km	Manning's n	WS Slope	d <sub>50j</sub> (mm)	Tau <sub>c</sub> *	Sort
Bend Bridge	23051	418.9	0.035	0.00131	9.50	0.053	2.493
Hamilton Cty	28645	320.7	0.035	0.00026	4.00	0.136	2.300
Butte Cty	31274	271.2	0.035	0.00050	2.50	0.133	2.598
Colusa	31313	231.1	0.035	0.00009	0.42	0.429	2.055
Knights Lndg	37645	144.2	0.035	0.00011	0.35	<b>0.429</b>	2.436
Sacramento	60886	96.0	0.030	0.00003	0.03	<b>0.429</b>	0.985
Cottonwood	2401	-	-	-	2.50	0.013	1.790
Cow	1101	-	-	-	10.00	0.11	2.993
Thomes	736	-	-	-	4.50	0.012	1.807
Feather	2065	-	-	-	0.35	<b>0.429</b>	0.700

**Table 3.1** Station, drainage area, river kilometer, Manning's n, water surface slope (for baseline conditions),  $d_{50j}$ , and  $\tau_c^*$  and sorting coefficient. The bold figures in the  $\tau_c^*$  column represent stations for which no bedload data were available. I simply applied the  $\tau_c^*$  from Colusa to compute bed-material load at these stations.